LOCALLY OPTIMUM AND SUBOPTIMUM DETECTOR PERFORMANCE IN A NON-GAUSSIAN INTERFERENCE ENVIRONMENT

A. D. Spaulding*

Since the normally assumed white Gaussian interference is the most destructive in terms of minimizing channel capacity, substantial improvement can usually be obtained if the real-world interference environment (non-Gaussian) is properly taken into account. In this report, the performance of the locally optimum Bayes detector (LOBD) is compared with the performance of various ad hoc nonlinear detection schemes. The known results are reviewed and then it is demonstrated that these theoretical results may be misleading due to the assumptions that are required in order to derive them analytically. For a particular type of broadband impulsive noise, the critical assumptions of "sufficiently" small signal level and large number of samples (large time-bandwidth product so that the Central Limit Theorem applies) are removed; the first, analytically, and the second, by computer simulation. The thus derived performance characteristics are then compared, especially as the signal level increases. One result is that there are situations where the bandpass limiter outperforms the LOBD as the signal level increases; that is, the locally optimum detector may not remain "near optimum" in actual operational situations.

Key words: optimum detection; non-Gaussian noise; communication system simulation; parametric signal detection; Class A, B noise

1. INTRODUCTION

The real-world noise environment is almost never Gaussian in character, yet receiving systems in general use are those which are optimum for white Gaussian noise (i.e., linear matched filter or correlation detectors).

It is well known that Gaussian noise is the worst kind of noise in terms of minimizing channel capacity or in its information destroying capability. This means that very large improvements in the performance of systems can be achieved if the actual statistical characteristics of the noise and interference are properly taken into account, and there have been various significant efforts in the last few years in this area (Spaulding and Middleton, 1977; Middleton and Spaulding, 1983).

When confronted with real-world noise, the earlier and usual approach was to precede the "Gaussian receiver" by various ad hoc nonlinearities (e.g., clipper, hole punchers, hard limiters, etc.) in order to make the noise look "more Gaussian" to the given receiver. Later, optimum systems were derived (e.g., Spaulding and Middleton, 1977; Hall, 1966) using models of the actual noise. These systems are

*The author is with the U. S. Department of Commerce, National Telecommunications and Information Administration, Institute for Telecommunication Sciences, Boulder, Colorado 80303.

adaptive in nature and usually very difficult to realize physically. If, however, the following two assumptions are made:

1) the desired signal becomes "sufficiently" small ["sufficiently small" is defined in Middleton and Spaulding (1983)*], and
2) the time-bandwidth product is large, so that a large number, N, of independent samples from the interfering noise process can be used in the detection decision process,

then a "locally optimum" detector, generally termed a "locally optimum Bayes detector" or LOBD, can be obtained. Under some rather strict conditions, these LOBD detectors approach true optimality (asymptotically) as the above two assumptions are met, and usually take the form of the "normal" Gaussian receiver preceded by one or more particular nonlinearities.

In this report, we want to briefly review the derivation of the LOBD, primarily for the case of binary coherent phase shift keying, CPSK, and then review the comparison of the LOBD performance with the performance of the hard-limiter (or other nonlinearity) performance. We do this to point out and have available the results we need to refer to later. In actual use, the desired signal may be "small," but not "small enough," and/or the time bandwidth product may not be particularly large. One of the main objectives, then, of this report is to remove the above two assumptions to investigate the "truth" of the standard LOBD and hard-limiter performance estimates. This is done for one typical example of broadband impulsive noise. For this example case, the first assumption (sufficiently small signal) is removed analytically and the second (large N so that Central Limit Theorem arguments can be used) is removed by computer simulation. Another main objective of this report is to summarize the results from an extensive set of Monte Carlo computer simulation results for the CPSK system, using various nonlinearities (including the LOBD nonlinearity) and also using Rayleigh fading signals as well as constant signals. We start in the next section by reviewing the pertinent standard analytical results for the LOBD and then proceed to remove the assumptions used to obtain the "standard" performance estimates. An appendix contains the computer algorithms used to obtain the Monte Carlo simulation results.

---

*See Sections 2.4, 6.4, and Appendix A.3 of Middleton and Spaulding (1983).

2. LOCALLY OPTIMUM DETECTION

The techniques for deriving the locally optimum detector for various signaling situations are well known and covered in detail in Spaulding and Middleton (1977) and the references therein. Here, we simply review the results in order to indicate where the two assumptions above come into play. Our problem, for binary CPSK, is to decide optimally between the two hypotheses:

$$\begin{aligned} H_1 &: \quad X(t) = S_1(t) + Z(t) \qquad 0 \leq t < T \\ H_2 &: \quad X(t) = S_2(t) + Z(t) \qquad 0 \leq t < T. \end{aligned} \tag{1}$$

In (1), $X(t)$ is our received waveform in detection time T and this waveform contains either the completely known signal $S_1(t)$ plus the noise $Z(t)$ or the completely known, equi-probable, signal $S_2(t)$ plus $Z(t)$. To obtain our receiver structure we follow the standard procedure of replacing all waveforms by vectors of N samples from the waveforms ($X(t) \rightarrow \underline{X} = \{x_i\}$, etc.) and forming the likelihood ratio $\Lambda(\underline{X})$:

$$\Lambda(\underline{X}) = \frac{p(\underline{X}|H_2)}{p(\underline{H}|H_1)} = \frac{p_Z(\underline{X} - \underline{S}_2)}{p_Z(\underline{X} - \underline{S}_1)} \underset{H_2}{\overset{H_1}{\lesssim}} 1. \tag{2}$$

When $Z(t)$ is non-Gaussian, we operate so as to generate independent noise samples, z_i, $i = 1, N$ in time T, so that only first order pdf's are required. We now use the LOBD or threshold operation which we know becomes asymptotically optimum as our signal $S(t)$ becomes sufficiently small and $N \rightarrow \infty$ (Middleton and Spaulding, 1983). Increasing N corresponds to increasing the detection time T, since we cannot for any noise process sample more rapidly than the bandwidth and maintain independence. Using a vector Taylor expansion about the signals, $\underline{S}_j$, $j = 1, 2$ here, we get

$$\begin{aligned} p_Z(\underline{X} - \underline{S}_j) = p_Z(\underline{X}) &- \sum_{i=1}^{N} \frac{\partial p_Z(\underline{X})}{\partial x_i} S_{ji} \\ &+ \frac{1}{2} \sum_{i=1}^{N} \sum_{k=1}^{N} \frac{\partial^2 p_Z(\underline{X})}{\partial x_i \, \partial x_k} S_{ji} S_{jk} + \cdots \end{aligned} \tag{3}$$

In this expansion, for coherent signaling, all signal terms of degree two and higher are discarded. This is the normal "small signal assumption." In general, simply discarding higher order terms can lead to receiver structures which are not locally optimum, or in the limit of infinitely large sample sizes ($N \to \infty$), are not asymptotically optimum detection algorithms (AODA's). The proper algorithms require a correct bias (obtainable from proper treatment of the higher order terms)*. The problem is, that without the proper bias, the higher-order terms in the expansion of $\Lambda(\underline{X})$ can be discarded only when the sample size N is small. But N must be made large in order to obtain the required small probabilities of error for weak signals. This, of course, defeats the whole concept of a canonical and comparatively simple algorithm. One may as well use $\Lambda(\underline{X})$ itself, which is optimum for all signal levels. Sufficient conditions that the LOBD is an AODA as well as a LOBD ($N < \infty$) are given in Middleton and Spaulding (1983), Sec. A.3-3.

For binary symmetric CPSK, and for independent noise samples (3) leads to

$$\Lambda(\underline{X}) \sim \frac{1 - \sum_{i=1}^{N} \frac{d}{dx_i} \ell n\, p_Z(x_i) S_{2i}}{1 - \sum_{i=1}^{N} \frac{d}{dx_i} \ell n\, p_Z(x_i) S_{1i}} \underset{H_2}{\overset{H_1}{\lessgtr}} 1, \tag{4}$$

which gives the well-known receiver structure shown in Figure 1. In Figure 1, we see that the receiver is the standard memoryless Gaussian (i.e., degenerate matched filter) preceded by a particular nonlinearity given by

$$\ell(x) = - \frac{d}{dx} \ell n\, p_Z(x) \; . \tag{5}$$

Note that this is a completely canonical result in that we have not yet specified (in the above derivation) what $p_Z(z)$ is or what the signals $S_1(t)$, $S_2(t)$ are except that they are completely known. Figure 1 is our receiver, which is adaptive in that it must change according to (5) for changing noise conditions. The receiver takes our received waveform samples x_i and uses them as shown to determine our decision variable δ. Now, in order to determine performance we need the pdf of δ. The pdf of δ is almost always impossible to obtain, however, unless we can invoke the Central Limit Theorem.

* For cases of threshold signal detectors that are neither locally optimum or asymptotically optimum detection algorithms, see Lu and Eisenstein (1981).

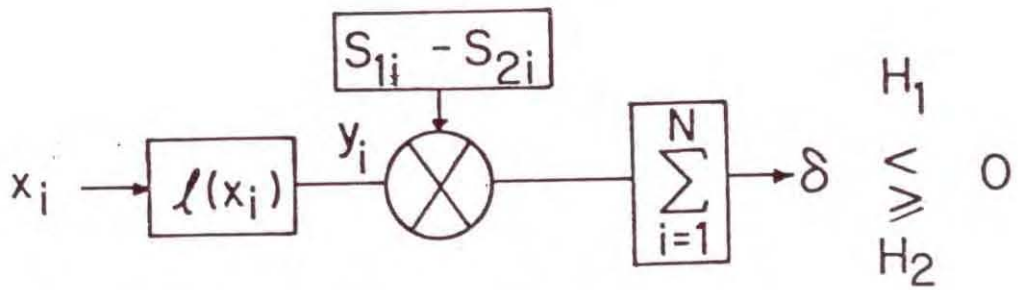

Figure 1. LOBD for binary symmetric purely coherent signals.

Although the nonlinearity $\ell(x)$ does not "Gaussianize" the noise, it does limit the amplitude excursions of the noise. Because of this, it is common to require N to be large (normally N must be relatively large to achieve any kind of processing gain over normal receivers as will be demonstrated later via simulation) so that we can apply the Central Limit Theorem. This means that we only need to compute the mean and variance of δ under each of the two hypotheses. We start with y_i, the output of the nonlinearity for input x_i. Suppose H_1 is true, then

$$E[y_i|H_1] = -\int_{-\infty}^{\infty} \frac{p_Z'(z)}{p_Z(z)}\, p_Z(z - S_{1i})\, dz. \tag{6}$$

and

$$E[y_i^2|H_1] = \int_{-\infty}^{\infty} \left[\frac{p_Z'(z)}{p_Z(z)}\right]^2 p_Z(z - S_{1i})\, dz\ .$$

In evaluating the above two integrals, the usual approach is to expand the $p_Z(z - S_{1i})$ and then discard all terms in S_{1i} of degree 2 and higher. (As mentioned earlier, one of the objects is to investigate the effect of using this small signal assumption this second time.) Doing the above, we obtain

$$E[y_i|H_1] \doteq -S_{1i}L, \text{ where} \tag{7}$$

$$L = \int_{-\infty}^{\infty} \frac{[p_Z'(z)]^2}{p_Z(z)}\, dz, \text{ and} \tag{8}$$

$$E[y_i^2|H_1] \doteq L. \tag{9}$$

The parameter L determines (for "small"signal) the processing gain achievable for any $p_Z(z)$, including Gaussian noise (for which L = 1).

Using the above we obtain, for binary symmetric signal with $S_1(t) = -S_2(t)$ (CPSK),

$$E[\delta|H_2] = -E[\delta|H_1] = 2L \sum_{i=1}^{N} S_{1i}^2 \text{ , and} \tag{10}$$

$$\text{Var}[\delta|H_2] = \text{Var}[\delta|H_1] = 4 \sum_{i=1}^{N} (LS_{1i}^2 - L^2 S_{1i}^4).$$

An estimate of performance is then given by

$$P_e = \text{Prob}[\delta < o] = \frac{1}{2} \text{ erfc } \left\{ \frac{|E[\delta]|}{\sqrt{2\text{Var}[\delta]}} \right\} . \tag{11}$$

If our two signals are, for example,

$$S_1(t) = \sqrt{2S}\cos(\omega_o t), \qquad 0 \leq t < T$$

and $\tag{12}$

$$S_2(t) = -\sqrt{2S}\cos(\omega_o t), \qquad 0 \leq t < T$$

so that S is the signal power, then

$$E[\delta] = 2SLN, \text{ and} \tag{13}$$

$$\text{Var}[\delta] = 4SLN - 6S^2L^2N. \tag{14}$$

Since all our noise models are normalized so that the noise power = 1, S is also our signal-to-noise ratio. We note that SL must be such that the variance is positive. Since L is usually large (i.e., $\sim 10^3 - 10^4$), (14) defines, in a sense, the meaning of "small" signal in the above LOBD analysis. [Very detailed definitions of "small signal" are given in Middleton and Spaulding (1983), cf. Sections 7.4,A.3.] If SL << 1, then (11) becomes approximately

$$P_e \overset{\sim}{=} 1/2 \text{ erfc } (\sqrt{SNL/2}) \quad . \tag{15}$$

For LOBD's, the performance parameter L is ≥ 1, and is equal to 1 iff the noise is Gaussian.

The above reviews the LOBD approach. Suppose now that we have a LOBD detector based on the assumption that our interference is $\hat{p}_Z(z)$, and the actual interference is $p_Z(z)$. We can carry out the above analysis using $\hat{p}_Z(z)$ in place of $p_Z(z)$ where appropriate to determine the effects of "mismatching" the interference, or we can use this to determine the sensitivity of the LOBD performance to changing interference. This approach also gives results which can be easily used to evaluate the small signal performance of any ad hoc nonlinearity. The result is that L is replaced by a parameter L_{eff}, for "L effective," where, $L_{eff} = L_1^2/L_2$,

$$L_1 = \int_{-\infty}^{\infty} \left[\frac{\hat{p}_Z'(z)}{\hat{p}_Z(z)} \right] p_Z'(z)dz, \quad \text{and} \tag{16}$$

$$L_2 = \int_{-\infty}^{\infty} \left[\frac{\hat{p}_Z'(z)}{\hat{p}_Z(z)} \right]^2 p_Z(z)dz \ . \tag{17}$$

If $\hat{p}_Z(z) = p_Z(z)$, then $L_1 = L_2 = L = L_{eff}$.

We can quickly compute the performance of any arbitrary nonlinearity, $\ell(x)$, used in the detector of Figure 1. For example, for the hard-limiter, $\ell(x) = 1$, if $x \geq 0$ and $\ell(x) = -1$, if $x < 0$. We can solve the resulting expression

$$\ell(x) = - \frac{d}{dx} \ell n \ \hat{p}_Z(x) \ , \tag{18}$$

to obtain the corresponding $\hat{p}_Z(z)$ to compute L_{eff} via (16) and (17) above. For the hard-limiter case, we obtain

$$L_{eff} = 4 \ p_Z^2(0). \tag{19}$$

where $p_Z(z)$ is the actual interference. Performance is given by (15), so that the degradation caused by using the hard-limiter is simply the difference between L for our actual interference (LOBD performance factor) and L_{eff} for the hard-limiter (or similarly, for any other nonlinearity).

Up to this point, we have not specified any "model" for the real world non-Gaussian noise and interference environment. Recent work by Middleton has led to the development of a physical-statistical model for radio noise. This model has been used to develop optimum detection algorithms for a wide range of communications problems (Spaulding and Middleton , 1977). It is this model which we use here for our signal detection problem. The Middleton model is the only general one proposed to date in which the parameters of the model are determined explicitly by the underlying physical mechanisms (e.g., source density, beam-patterns, propagation conditions, emission waveforms, etc.). It is also the first model which treats narrowband interference processes (termed Class A), as well as the traditional broadband processes (Class B). The model is also canonical in nature in that the mathematical forms do not change with changing physical conditions. For a large number of comparisons of the model with measurements and for the details of the derivation of the model, see Middleton (1977,1983) and Spaulding (1977). We only summarize the results of the model which we need here.

For our received noise process Z(t), the probability density function (pdf) for the received instantaneous amplitude, z, is:

$$p_Z(z) = \frac{e^{-z^2/\Omega}}{\pi\sqrt{\Omega}} \sum_{m=0}^{\infty} \frac{(-1)^m}{m!} A_\alpha^m \Gamma\left(\frac{m\alpha+1}{2}\right) {}_1F_1\left(-\frac{m\alpha}{2}\,;\, 1/2;\, \frac{z^2}{\Omega}\right) \quad , \qquad (20)$$

$$-\infty \leq z \leq \infty$$

where ${}_1F_1$ is a confluent hypergeometric function. The model has three parameters: α, A_α, and Ω. [A more detailed and complete model involving additional parameters has been developed, but (20) above is quite sufficient for our purposes]. The parameters α and A_α are intimately involved in the physical processes causing the interference. Again, definitions and details are contained in the references. The parameter Ω is a normalizing parameter. In the references, the normalization is $\Omega = 1$, which normalizes the process to the energy contained in the Gaussian portion of the noise. Here we use a value of Ω which normalizes the process (z values) to the measured energy in the process. We cannot normalize to the computed energy, since for (1), the second moment (or any moment) does not exist (i.e., is infinite). This is a typical problem with most such models for broadband impulsive noise. While the more complete model removes this problem, use of (20) in conjunction with measured data, will in no way limit us. However, when we discuss the simulation results, we will see an interesting result of using "infinite energy" models.

The result corresponding to (20) for the envelope cumulative distribution (APD) is:

$$P(E > E_o) = e^{-E_o^2/\Omega}\left[1 - \frac{E_o^2}{\Omega}\sum_{m=1}^{\infty}\frac{(-1)^m}{m!}A_\alpha^m\right. \tag{21}$$

$$\left. \times\, \Gamma\left(1 + \frac{m\alpha}{2}\right){}_1F_1\left(1 - \frac{m\alpha}{2};\ 2;\ \frac{E_o^2}{\Omega}\right)\right]$$

$$0 \leq E \leq \infty \ .$$

It is the envelope distribution in the above form which is usually measured and which we use for validation of the model by comparison with measurements.

The corresponding expressions for the Class A, narrowband "impulsive" noise are

$$P_Z(z) = e^{-A}\sum_{m=0}^{\infty}\frac{A^m}{m!\sqrt{2\pi\sigma_m^2}}\,e^{-z^2/2\sigma_m^2}\ , \tag{22}$$

where

$$\sigma_m^2 = \frac{m/A + \Gamma'}{1 + \Gamma'}\ , \tag{23}$$

and, for the envelope,

$$P(E > E_o) = e^{-A}\sum_{m=0}^{\infty}\frac{A^m}{m!}\,e^{-E_o^2/\sigma_m^2}\ . \tag{24}$$

The Class A model has two parameters: A and Γ'. A is termed the overlap index, and as A becomes large ($\sim$10), the noise approaches Gaussian (still narrowband) and Γ' is the ratio of the energy in the Gaussian portion of the noise to the energy in the non-Gaussian component.

The Class A model is appropriate for interference caused by collections of intentionally-radiated signals (e.g., as in the crowded HF band) and has also found

application in various acoustical (e.g., sonar) problems. The Class B model is appropriate for broadband impulsive noise processes such as atmospheric noise, automotive ignition noise, etc.

Figures 2 and 3 show the comparison of the limiting small signal performance for the LOBD with the corresponding performance for the hard limiter. Figure 2 is for the Class B Middleton model for a wide range of the parameters α and A_α, and Figure 3 is for the Class A model for various values of the parameters A and Γ'. A couple of example values for L are also shown on the figures. On Figure 2, the point shown ($\alpha = 1$, $A_\alpha = 1$) will be used and referred to later.

While the hard-limiter may not be the suboptimum nonlinearity one would choose for all Class A cases, the results show that the Class A LOBD nonlinearity can substantially outperform the hard-limiter (Figure 3). The results for Class B noise would seem to indicate that one may as well use a hard-limiter rather than attempting to implement the much more difficult Class B LOBD nonlinearity. The results, however, are limiting results for a suitably small signal (>0) and $N \to \infty$.

Note that if we use the receiver optimum for Gaussian noise (no nonlinearity), the limiting performance ($N \to \infty$) is identical for all types of noise (i.e., $L_{eff} = 1$ from (16) and (17) for <u>any</u> $p_Z(z)$). While this is certainly true in the limit, we also know that performance of systems, using the Gaussian receiver in non-Gaussian noise, can be quite different, even for very small signals. This means that, in this case at least, the limiting performance may not give a good estimate for real-world small signal situations, especially for relatively small N. For large N, and any noise process, we expect the performance to approach the same characteristic performance as for Gaussian noise due to the Central Limit Theorem. However, we have no means of locating this "Gaussian performance curve" in terms of signal-to-noise ratio. [For our CPSK case, we will see that the parameter L is a measure of the difference (in the limit as $N \to \infty$) between the LOBD "Gaussian performance curve" and the linear receiver "Gaussian performance curve," where both are operating in the same non-Gaussian noise environment.] Figure 2 shows that the Class B LOBD nonlinearity and the hard-limiter nonlinearity behave similarly (only small degradation); however, these results may be true only in the limit. In the next section, we investigate this question.

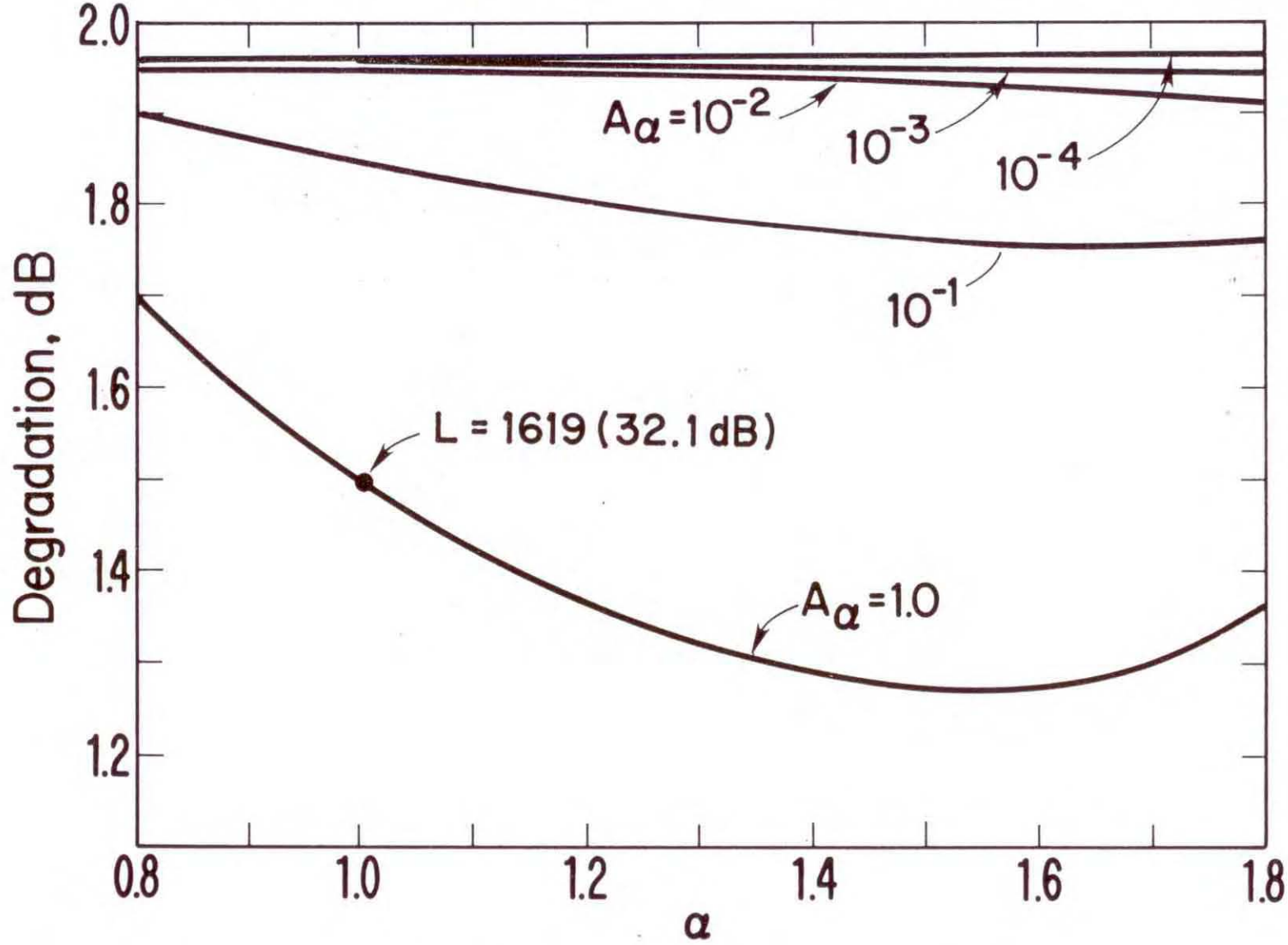

Figure 2. Comparison of the optimum nonlinearity for Class B noise with the hard-limiter.

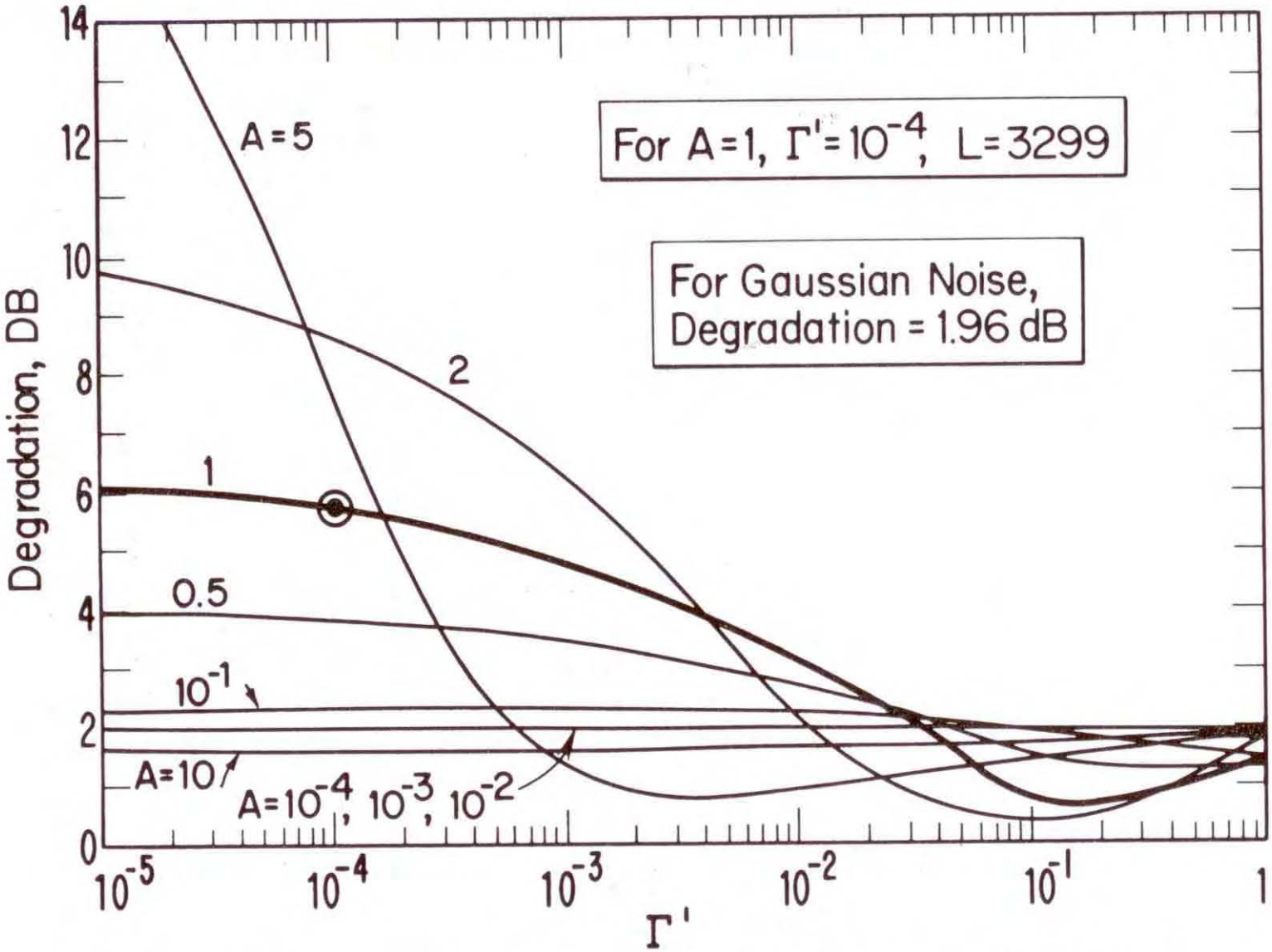

Figure 3. Comparison of the optimum nonlinearity for Class A noise with the hard-limiter.

3. REMOVAL OF ASSUMPTIONS

In the last section, the performance of the LOBD and various suboptimum nonlinearities (e.g., the hard limiter) was evaluated using the Central Limit Theorem in that only the mean and variance of the detection variable δ needed to be evaluated and also using the sufficiently small signal assumption to then evaluate the required integrals (6). We now want to remove these assumptions to see what effect they may have on estimating the performance of actual systems.

There are two possible approaches. The first is direct computer simulation to obtain Monte Carlo performance results comparing the various nonlinearities. The Middleton models are such that it would be difficult to rapidly generate the random noise samples required. The second approach is to use the Central Limit Theorem, but evaluate the integrals (6) directly without the small signal assumptions. This is also a formidable task, in general, due to the mathematical complexity of the noise models. There is one Class B situation, however, where both the above methods can be used. For Class B noise with $\alpha = 1$, Middleton (1976) has shown that the model (20) reduces to the following,

$$p_Z(z) \simeq \frac{2A_\alpha \sqrt{\Omega}}{\pi(4z^2 + \Omega A_\alpha^2)} \quad , \tag{25}$$

with the corresponding envelope APD given by

$$p(E > E_o) \simeq \frac{1}{\sqrt{1 + 4E_o^2/\Omega A_\alpha^2}} \quad . \tag{26}$$

The expressions above are models of the Hall (1966) type (Hall parameter $\theta = 2$), so the Middleton models can give some physical basis for the Hall model. The above [(25) and (26)] are only good approximations at the high amplitude "tails" and then only for relatively large values of $A_\alpha (A_\alpha \geq 1)$. Figure 4 shows the Hall model envelope distribution from (26) and the Middleton envelope distribution from (21) for $\alpha = 1$ and $A_\alpha = 1$. Also shown on Figure 4 is the Middleton model for $\alpha = 1$ and $A_\alpha = 10^{-3}$. As can be seen, the approximation given by (26) is only valid for large amplitudes and that (26) can be used to approximate the entire distribution only for the larger values of A_α. We are, of course, assuming that the physical-statistical model of Middleton is the appropriate model to "match" the actual environment (this has been reasonably well substantiated) and are using the Hall model

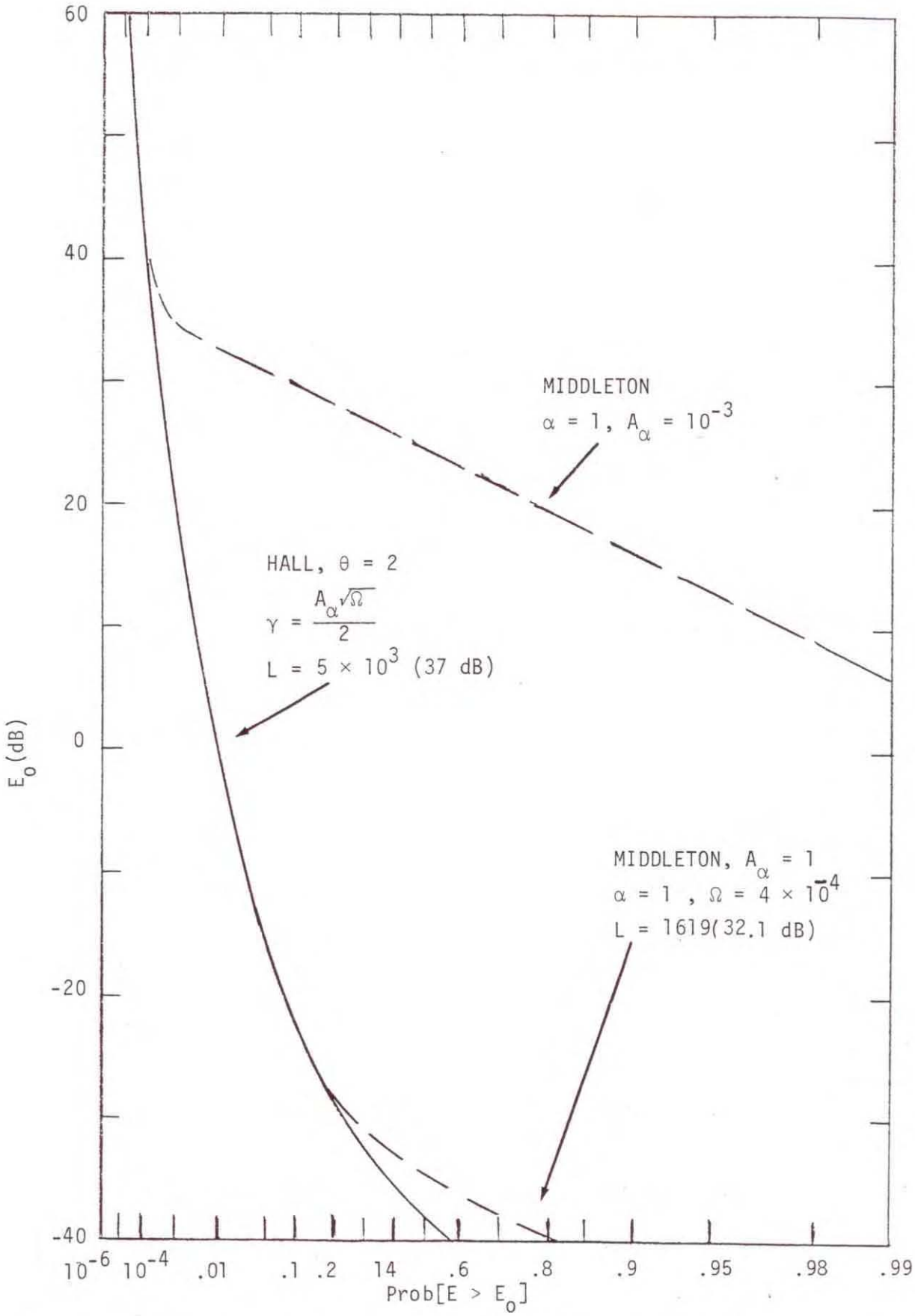

Figure 4. Comparison of the Middleton model for $\alpha = 1$ and $A_\alpha = 1$ and 10^{-3} with the Hall model, $\theta = 2$.

via (25) and (26) to obtain a simple mathematical form for a special case of Middleton's model.

For the Middleton model ($\alpha = 1$, $A_\alpha = 1$), L = 32.1 dB (Figure 2). The general Hall model has two parameters, θ and γ, and is given by

$$p_Z(z) = \frac{\Gamma\left(\frac{\theta}{2}\right)\gamma^{\theta-1}}{\Gamma\left(\frac{\theta-1}{2}\right)\sqrt{\pi}\left[z^2+\gamma^2\right]^{\theta/2}} \tag{27}$$

For $\theta = 2$ and $\gamma = A_\alpha\sqrt{\Omega}/2$, the Middleton approximation (25) is obtained. The corresponding general Hall APD form is

$$P[E > E_o] = \frac{\gamma^{\theta-1}}{\left(E_o^2+\gamma^2\right)^{(\theta-1)/2}} \quad . \tag{28}$$

When (27) is used in the "L integral" (8), we obtain

$$L = \frac{\theta^2\Gamma\left(\frac{\theta}{2}\right)\gamma^{\theta-1}}{\Gamma\left(\frac{\theta-1}{2}\right)\sqrt{\pi}} \int_{-\infty}^{\infty} \frac{z^2}{\left(z^2+\gamma^2\right)^{\frac{\theta}{2}+2}}\, dz \quad . \tag{29}$$

The parameter γ is a "normalizing parameter" equivalent to Ω in the Middleton model. For our case ($\alpha = 1$, $A_\alpha = 1$), $\gamma = \sqrt{\Omega}/2$. For $\theta = 2$, (29) then gives

$$L = 2/\Omega \quad . \tag{30}$$

The parameter Ω is defined as $2/(\text{envelope rms})^2$ (since the envelope power is twice the actual noise power), and the envelope rms must be computed from the model. In obtaining the results of Figure 2, the Middleton model was assumed to saturate at 80 dB above the Gaussian level or at an exceedance probability of 10^{-6}, whichever came first. That is, we must use a truncated model since the rms for the actual model does not exist. For the Middleton model ($A_\alpha = 1$, $\alpha = 1$), this gives $\Omega = 3.99959 \times 10^{-4}$. For the corresponding Hall model (for any large truncation point), we obtain for $\theta = 2$ and truncation at 80 dB, corresponding to the Middleton example,

$$0.5 \times (\text{Envelope rms})^2 = \frac{1}{2}\gamma \int_0^{10^4} \frac{E^2}{(E^2 + \gamma^2)^{3/2}}\, dE = 1 , \qquad (31)$$

or $$\gamma = \sqrt{2} \times 10^{-2} ,$$

resulting in [from (26) and (28)] $\Omega = 4 \times 10^{-4}$, almost precisely the normalization value obtained earlier for the Middleton example. Therefore, for the Hall model, $\theta = 2$, properly normalized, $L = 5 \times 10^3$ or 37 dB. For the Middleton example, $L = 32.1$ dB and for the corresponding Hall model, $L = 37$ dB even though the impulsive tails are essentially identical. This points out that the value of L depends on the relationship between the low level Gaussian portion of the distribution and the rms level of the entire distribution. As can be seen from Figure 4, when the two distributions are "matched," the Hall distribution has a "lower" Gaussian level, resulting in a somewhat larger L. From now on, we will restrict our attention to (26), $L = 37$ dB (or $\Omega = 4 \times 10^{-4}$).

By using (25) for our pdf of the interfering noise, the integrals (6) can be directly integrated with no small-signal assumption. We obtain from (6) and (25)

$$E[y_i|H_1] = \frac{\sqrt{\Omega}}{\pi} \int_{-\infty}^{\infty} \frac{z}{\left(z^2 + \frac{\Omega}{4}\right)\left[\left(z - S_{1i}\right)^2 + \frac{\Omega}{4}\right]}\, dz , \qquad (32)$$

and

$$E[y_i^2|H_1] = \frac{2\sqrt{\Omega}}{\pi} \int_{-\infty}^{\infty} \frac{z^2}{\left(z^2 + \frac{\Omega}{4}\right)^2\left[\left(z - S_{1i}\right)^2 + \frac{\Omega}{4}\right]}\, dz . \qquad (33)$$

The two integrals are most easily evaluated by contour integration using residues. After a rather extensive amount of algebra, we obtain

$$E[y_i|H_1] = \frac{2S_{1i}}{S_{1i}^2 + \Omega} \quad , \tag{34}$$

and

$$E[y_i^2|H_1] = \frac{2(3S_{1i}^2 + \Omega)}{(S_{1i}^2 + \Omega)^2} \quad , \tag{35}$$

so that

$$Var[y_i|H_1] = \frac{2}{S_{1i}^2 + \Omega} \quad . \tag{36}$$

Therefore, for the detection variable δ (Figure 1),

$$E[\delta|H_1] = -E[\delta|H_2] = 4 \sum_{i=i}^{N} \frac{S_{1i}^2}{S_{1i}^2 + \Omega} \quad , \tag{37}$$

and

$$Var[\delta|H_1] = Var[\delta|\ H_2] = 8 \sum_{i=1}^{N} \frac{S_{1i}^2}{S_{1i}^2 + \Omega} \quad . \tag{38}$$

Of course, for $S \to 0$, the above (37) and (38) reduce to the results obtained earlier (10) ($\Omega = 2/L$ and $LS << 1$).

The hard-limiter result obtained earlier (19), that is

$$L_{eff} = 4p_Z^2(0) \quad , \tag{39}$$

is a limiting result ($S \to 0$). For the Hall approximation (25)

$$L_{eff} = \frac{16}{\pi^2 \Omega} = 0.81\ L, \tag{40}$$

so for the Hall model the hard-limiter, according to (40), will result in 0.912 dB degradation, while for the corresponding Middleton model, the hard-limiter (in the limit) will result in a 1.5 dB degradation (Figure 2).

In terms of the actual signal samples, the suitably small signal approach gives

$$E[y_i|H_1] \doteq -2\, p_Z(0)\, S_{1i} \ , \tag{41}$$

so that for the detection variable δ,

$$E[\delta|H_1] = -E[\delta|H_2] \doteq \frac{8}{\pi\sqrt{\Omega}} \sum_{i=1}^{N} S_{1i}^2 \ , \tag{42}$$

and

$$Var[\delta|H_{1,2}] \doteq 4 \sum_{i=1}^{N} \left(S_{1i}^2 - \frac{16}{\pi^2\Omega} S_{1i}^4 \right) \ .$$

Without this small-signal assumption, the integrals (6) eventually give,

$$E[\delta|H_1] = E[\delta|H_2] = \frac{4}{\pi} \sum_{i=1}^{N} S_{1i}\, \mathrm{Tan}^{-1} \left(\frac{2\, S_{1i}}{\sqrt{\Omega}} \right) , \tag{43}$$

and

$$Var[\delta|H_{1,2}] = 4 \sum_{i=1}^{N} \left\{ S_{1i}^2 - \frac{4}{\pi^2} S_{1i}^2 \left[\mathrm{Tan}^{-1} \left(\frac{S_{1i}}{\sqrt{\Omega}} \right) \right]^2 \right\} .$$

Of course, as before as $S \to 0$, the results (43) approach those of (42). Also note that in (42) the variance quickly becomes negative as S increases, but in (43) the variance exists for all signal levels (but $\to 0$ as $S \to \infty$).

For the signaling set given by (12), we can generate our signal samples as follows:

$$S_1(t_i) = S_{1i} = \sqrt{2S} \cos \left[\frac{Q}{N-1} \cdot (i - 1) \right] \ , \tag{44}$$

where

$$t_i = \frac{T}{N-1} (i - 1) \qquad \text{and} \qquad Q = \omega_0 T \ .$$

We now use (44), (37,38), (42), or (43) in (11) to estimate performance for various signal-to-noise ratios S and number of samples N. (Also, for the coherent case considered here, it is just as valid to make all the signal samples the same, namely, $s_{1i} = \sqrt{S}$. In fact, this was done for the computer Monte Carlo simulations covered next.)

The comparison of the results using (44), (43), and (42) for N = 100 are shown in Figure 5. On Figure 5, three curves are given: the standard result ($S \to 0$) from (13,14), the result using (37,38) ($S \not\to 0$), and the hard limiter result from (43) ($S \not\to 0$). The signal samples were generated via (44). Also shown on Figure 5 are simulation results (to be covered in the next section) for the LOBD nonlinearity (bandpass) and the bandpass limiter, and we see that the calculated results are quite close to the simulated results in all cases. Note that removing the small signal assumption makes only about 1.5 dB difference (the same is true for the hard-limiter). Since N = 100 here, we expect the Central Limit Theorem approximation to be quite adequate, and we see that it is.

Figure 6 shows results for N = 10. First, we note that performance cannot be calculated from the normal result (13,14) since the variance quickly becomes negative. This is noted by the dashed curve ($S \to 0$). The hard-limiter calculation from (43) ($S \not\to 0$) matches the simulation results only for small signal levels and departs rapidly as the signal increases. The LOBD calculated results from (37,38) ($S \not\to 0$) follow the simulated results better. The differences are, of course, due to the Central Limit Theorem approximation used for the calculated results not being valid for N = 10, especially in the "tails." The most interesting result shown, however, is that the hard-limiter outperforms the LOBD as the signal level increases (around SNR = -28 dB and $P_e = 10^{-6}$ in this case). Even though N = 10 and the simulation results go to $P_e = 10^{-6}$, the simulation results shown are statistically quite accurate. That is, the effect shown is real.

4. MONTE CARLO COMPUTER SIMULATION RESULTS

In the previous section, the assumption of suitably small signal normally used in performance estimation was removed for one Class B example. However, the Central Limit Theorem argument was still required. The only way to get around this, since it is impossible to find the actual pdf of the detection variable δ instead of just its mean and variance, is by direct computer simulation. This means that we must be able to quickly generate a large number of random samples from the appropriate noise and signal distributions. For example, if N = 100 and we want to determine performance in the range $P_e = 10^{-6}$ and we decide that we need at least ten

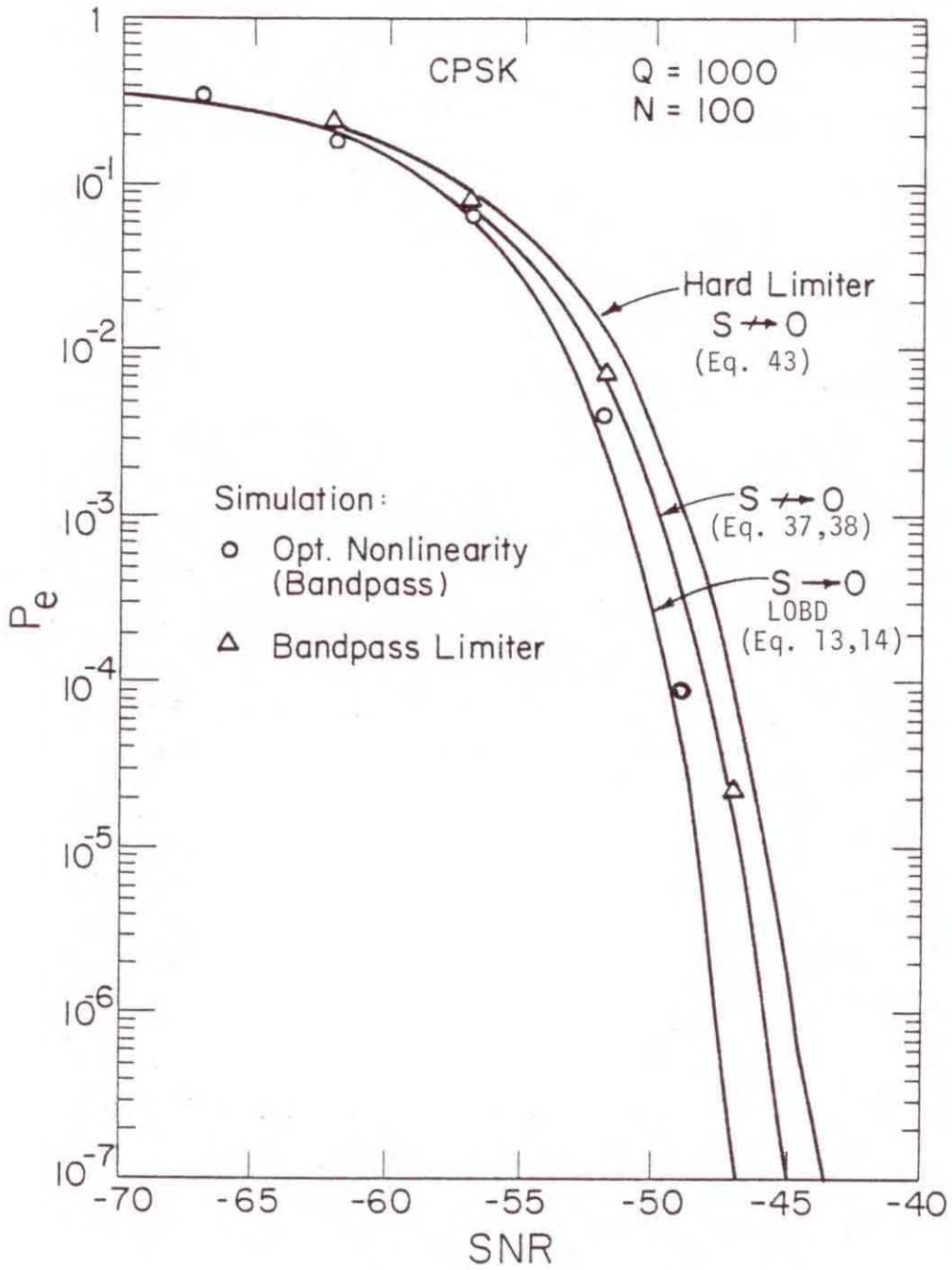

Figure 5. Calculated and simulation results for the hard-limiter and LOBD nonlinearities for N = 100.

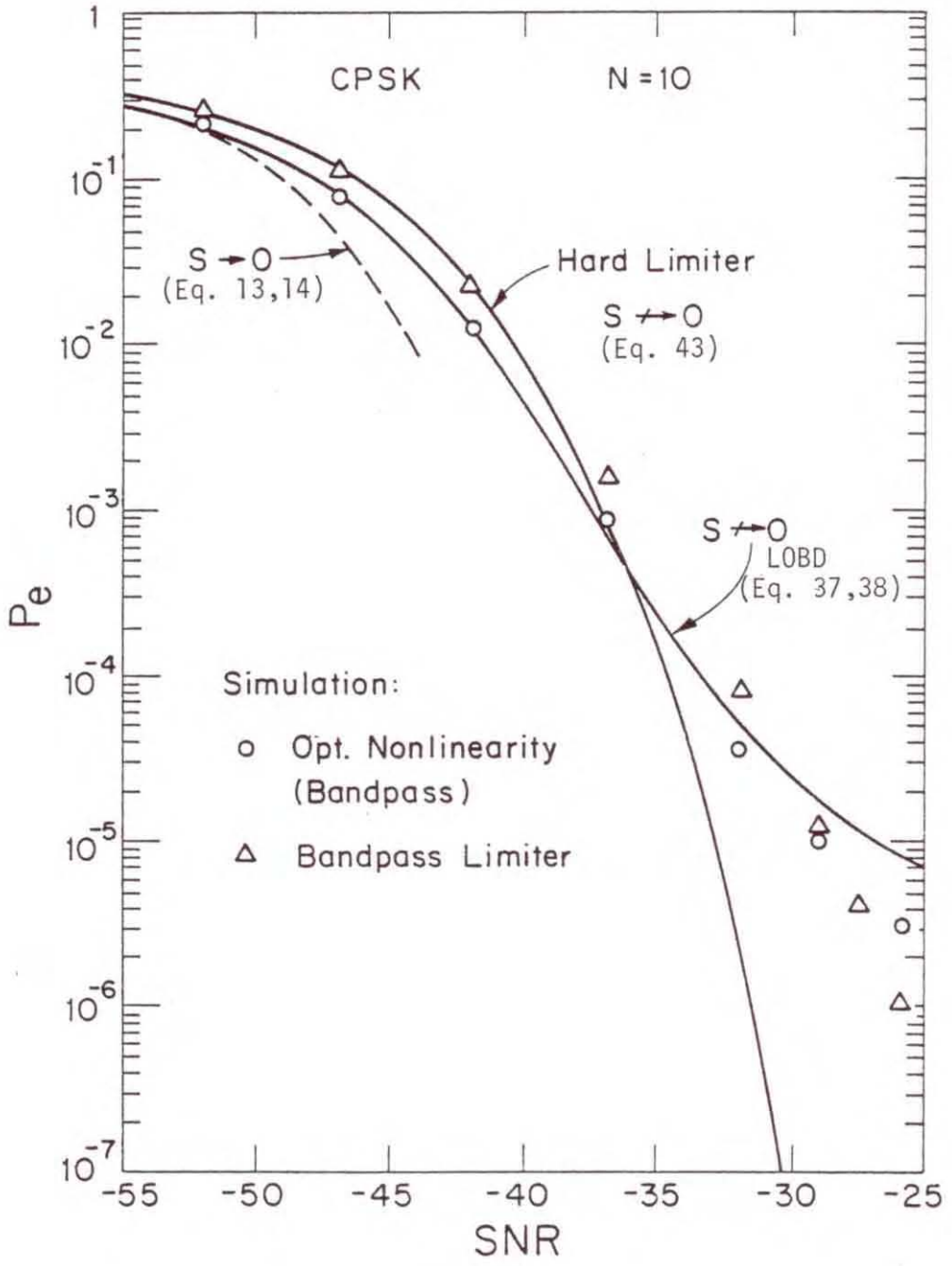

Figure 6. Calculated and simulation results for the hard limiter and LOBD nonlinearities for N = 10.

errors for statistical significance, then we need $100 \times 10 \times 10^6 = 10^9$ random samples for this one point. This problem of the large number of random samples required has always been one of the drawbacks of Monte Carlo simulation, and, obviously, the use of Middleton's model to generate random interference samples is out of the question without resorting to some much simpler approximation. It turns out that it is reasonably efficient to generate random noise samples from the Hall model.

In using Monte Carlo simulation, the accuracy of the estimate must be specified and this then usually determines the number of random samples required. A simple explanation of the Monte Carlo concept and various techniques has been given long ago by Kahn and Mann (1957) and an excellent survey has been presented by Halton (1970). Halton especially covers the important area of "variance reduction." The variance reduction technique appropriate to our problem is termed "Importance Sampling." The general idea of importance sampling is to draw samples from a distribution other than the one given by the problem and to carry along an appropriate weighting factor, which, when multiplied into the final results, corrects for having the wrong distribution. The biasing is done in such a way that the probability of the samples being drawn from an "interesting" region is increased. If good Importance Sampling techniques can be developed for a problem, then many less (orders of magnitudes less) random samples are required to achieve the same given level of statistical significance. Unfortunately, it is usually difficult to develop such techniques. A detailed example of using Importance Sampling quite effectively for nonlinear channels and Gaussian noise has been given by Shanmugam and Balaban (1980). Although substantial effort was expended, we could not develop any significantly "good" sampling methods for our problem at hand so that the results presented in this section are based on straight Monte Carlo techniques.

In generating the random samples in order to obtain the input x_i (Figure 1) to the system being simulated, bandpass processes are employed. That is, envelope and phase representations are used as in Figure 7. In Figure 7, the signal sample is $\sqrt{S}$, corresponding to the signals given by (12). Because of symmetry only $S_1(t)$ ($\sqrt{S}$) needs to be "sent." An error will occur whenever the resultant $\overline{X}_i$, after modification by the nonlinear receiver, lies in the shaded region of Figure 7. Actual detection is based on the sum of N such signal plus noise resultants. For a constant signal, all signal samples are the same, namely, the $\sqrt{S}$. Flat fading signal situations are obtained by using a constant signal throughout a detection interval T, but then allowing this "constant" to vary from one detection interval to the next according to some fading distribution. Results for flat Rayleigh fading

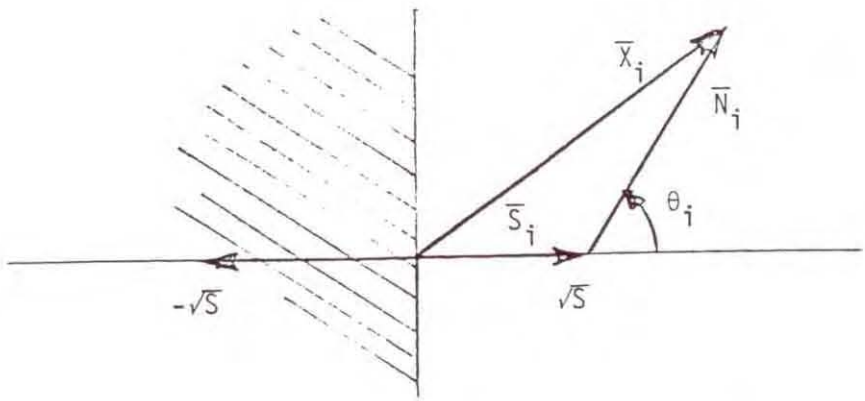

Figure 7. Signal phasors plus noise phasor for CPSK.

signals will be included here. Other fading situations can be simulated by allowing the signal samples to vary within a detection interval. On Figure 6, each noise sample $\overline{N}_i$ is obtained from the appropriate envelope (e.g., Rayleigh for Gaussian noise) and each noise phase angle, θ_i, is obtained from a uniform distribution $0 \leq \theta < 2\pi$.

The details of generating random samples from arbitrary distributions is treated by Bogdan (1981). The procedures start by generating a random sample (or samples) from a uniform distribution in the interval (0,1] and then modifying this sample according to the desired distribution. To do this usually requires taking the inverse of the cumulative distribution function (which, of course, makes it impossible to use Middleton's model). For example, for Gaussian noise, Rayleigh envelope, if V is uniform on (0,1], then a Rayleigh distributed random variable, X, is obtained from

$$X = [-2\,\sigma^2\,\ell n\,(1 - V]^{1/2}\,, \tag{45}$$

where σ^2 is the real noise power. If we have normalized the noise envelope to its rms value, i.e., envelope power = 1, then the real noise power, σ^2, is 1/2. For the Hall model, random samples are obtained from

$$X = \gamma(V^{\frac{-2}{\theta-1}} - 1)^{1/2}\,, \tag{46}$$

and we will give results for $\theta = 2$ (as in the last section) and for $\theta = 4$. Also, for the Hall model, the LOBD nonlinearity is quite simple (see Figure 1),

$$y_i = \frac{\theta x_i}{x_i^2 + \gamma^2} \quad . \tag{47}$$

In actual systems, the nonlinearity (47) operates on the magnitude of the complex received waveform sample, that is, the magnitude of $\overline{X}_i$ is used. In the hard limiter case, the bandpass version becomes a bandpass limiter. Physically, the bandpass limiter is a hard limiter followed by a zonal filter, so that no signal distortion is obtained from the nonlinearity and the following correlation receiver remains "matched" to the signal, as in the previous analysis. The behavior of the bandpass limiter when used with Gaussian noise and one CW signal has been analyzed in great detail by Davenport (1953) (see also problem 13, page 311 of Davenport and Root, 1958). A simplified analysis has also been given by Cahn (1961). This analysis shows that, in terms of signal-to-noise ratios (SNR) in and out of the nonlinearity.

$$\left(\frac{S}{N}\right)_o = \frac{\pi}{4}\left(\frac{S}{N}\right)_I \qquad \text{when } \left(\frac{S}{N}\right)_I << 1 \, ,$$

and (48)

$$\left(\frac{S}{N}\right)_o = 2\left(\frac{S}{N}\right)_I \qquad \text{when } \left(\frac{S}{N}\right)_I >> 1 \, .$$

That is, Gaussian noise and the bandpass limiter results in 1.05 dB degradation for small S/N and 3 dB degradation for large S/N. Using (19) to obtain L_{eff} for the hard-limiter and Gaussian noise, we obtain $L_{eff} = \pi/2 = 1.57$, or 1.96 dB degradation.

The receiver structures that were simulated are shown in Figure 8. The bandpass receivers (a,b,d, Figure 8) were used almost exclusively, but some results for the others (c and e, Figure 8) were obtained, mainly for curiosity's sake and to see how much difference resulted.

If the actual probability of error is P_e, then an estimate of P_e is

$$\hat{P}_e = \frac{1}{K} \sum_{i=1}^{K} a_i \, , \tag{49}$$

where a_i is 1 if the i^{th} transmitted symbol is in error and zero otherwise and K is the number of transmitted symbol with detection based on N sample points for each of the K symbols. The mean and variance of $\hat{P}_e$ are given by P_e and $P_e(1 - P_e)/K$,

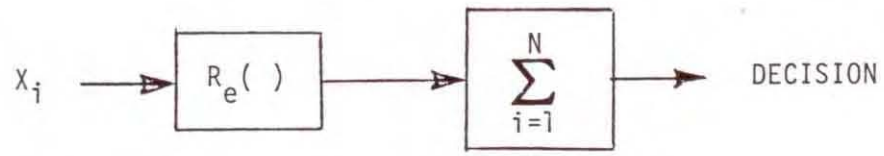

a) Linear Correlator Receiver

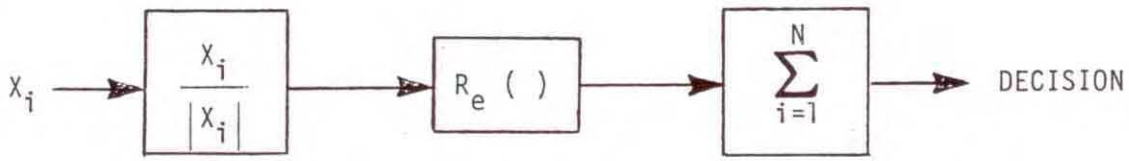

b) Bandpass Limiter Receiver

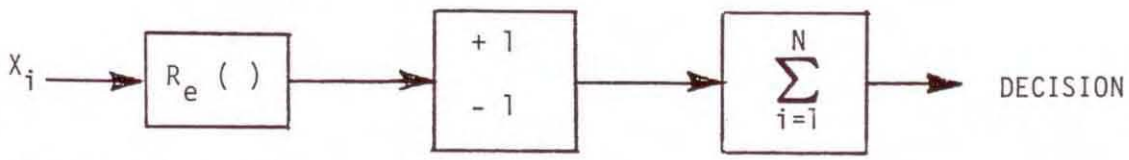

c) Hard-Limiter Receiver

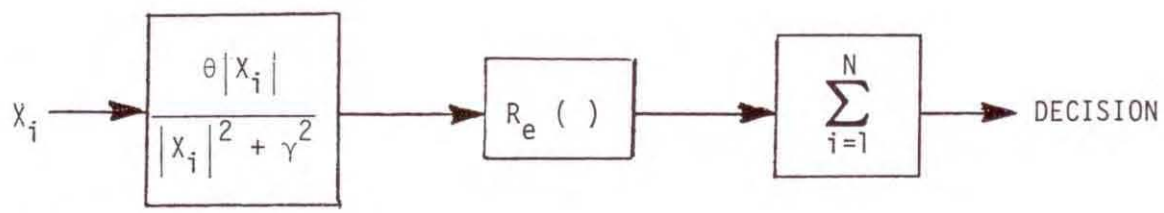

d) LOBD Bandpass Receiver

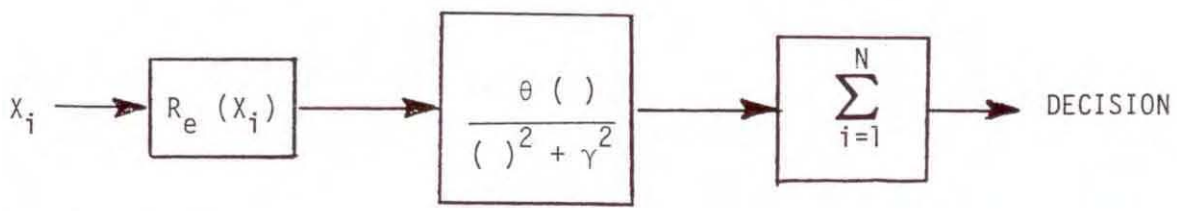

e) LOBD Receiver

Figure 8. Receiver structures.

respectively. For low probability of error, the normalized standard deviation is approximately $(KP_e)^{-1/2}$. The simulation programs are designed so that either a maximum number of symbols transmitted or a minimum number of errors detected will terminate the execution.

The first simulation results are given on Figure 9. These are for Gaussian noise for N = 1,10,100 using a linear receiver (optimum) and the hard-limiter [(c) of Figure 8] and the bandpass limiter. The object here is to make sure that the simulation results correspond to the known theoretical results so that we know the simulation programs are functioning properly. Results for a Rayleigh flat fading signal and Gaussian noise are also given on Figure 9 (N = 1). As expected, we see that the "hard limiter" is slightly inferior to the bandpass limiter.

Figure 10 shows results using the Hall model ($\theta = 2$) "normalized" as in the previous section to represent Middleton's model. The result from Figure 10 for N = 10 and 100 were discussed in the last section where they were compared to various analytical results. Note the interesting results for the linear receiver. Identical results were obtained for N = 1, 10, and 100. This is, of course, not physically meaningful and is the result of using a model for which the moments do not exist. This "infinite power" problem goes away whenever a nonlinearity is employed, as with the other results of Figure 10. For a linear receiver, for N = 10 say, detection is based on a "noise sample" which is the sum of the ten noise samples from the basic underlying distribution. Except for Gaussian noise, the distribution of the "sum sample" is different from the distribution of each individual sample, and approaches Gauss via the Central Limit Theorem. This makes it difficult to analytically determine the performance of linear systems in non-Gaussian noise for time bandwidth products other than 1. The above is for "real" noise processes with finite moments. Consider the Hall model for $\theta = 2$. The pdf is given by

$$p_Z(z) = \frac{\gamma}{\pi(z^2 + \gamma^2)} \quad , \tag{50}$$

so that the characteristic function is

$$\phi_Z(u) = \int_{-\infty}^{\infty} e^{-uz} \frac{\gamma}{\pi(z^2 + \gamma^2)} \, dy \tag{51}$$

This gives

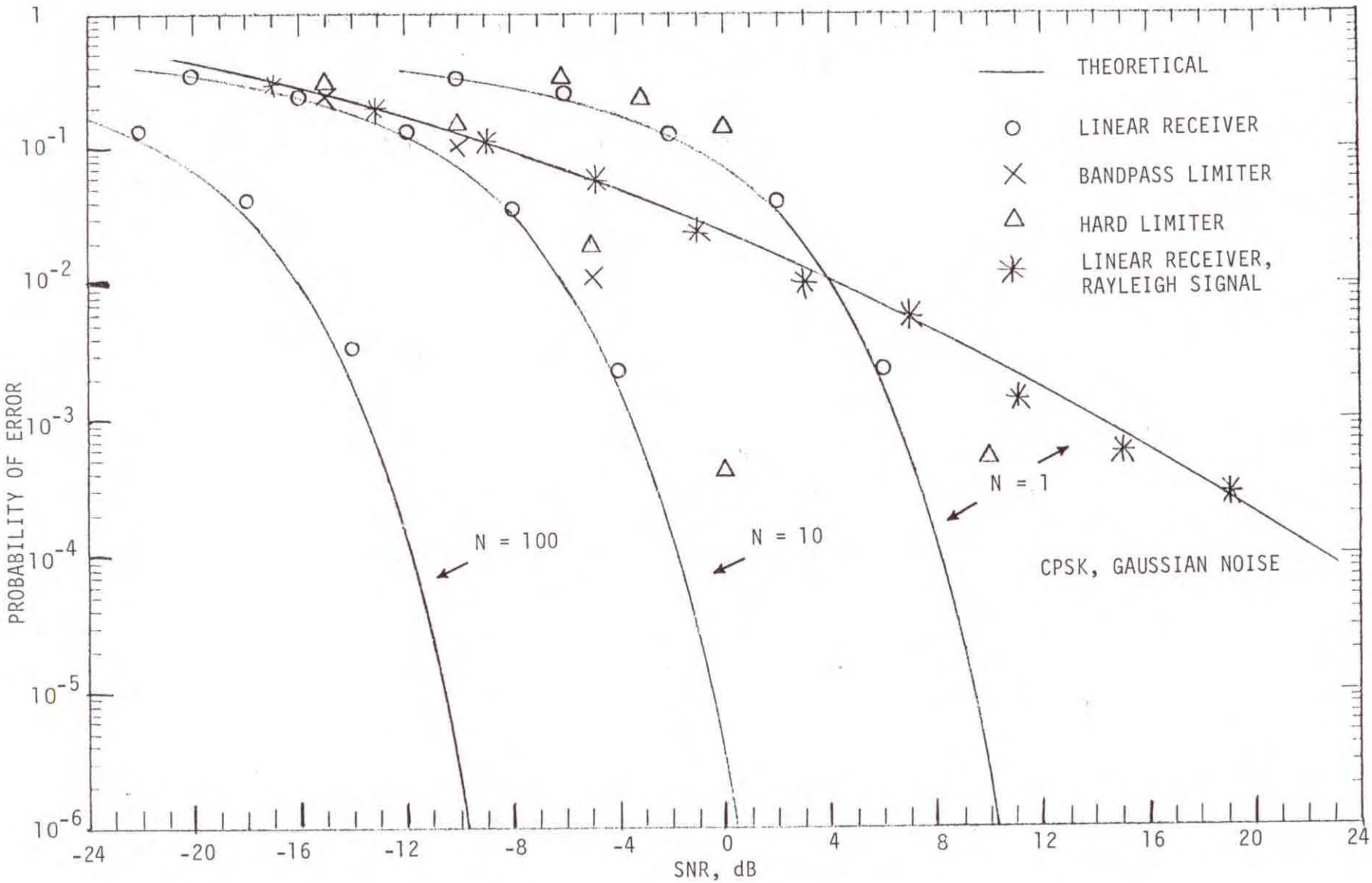

Figure 9. Simulation results with Gaussian noise for Rayleigh fading and constant signal for binary CPSK.

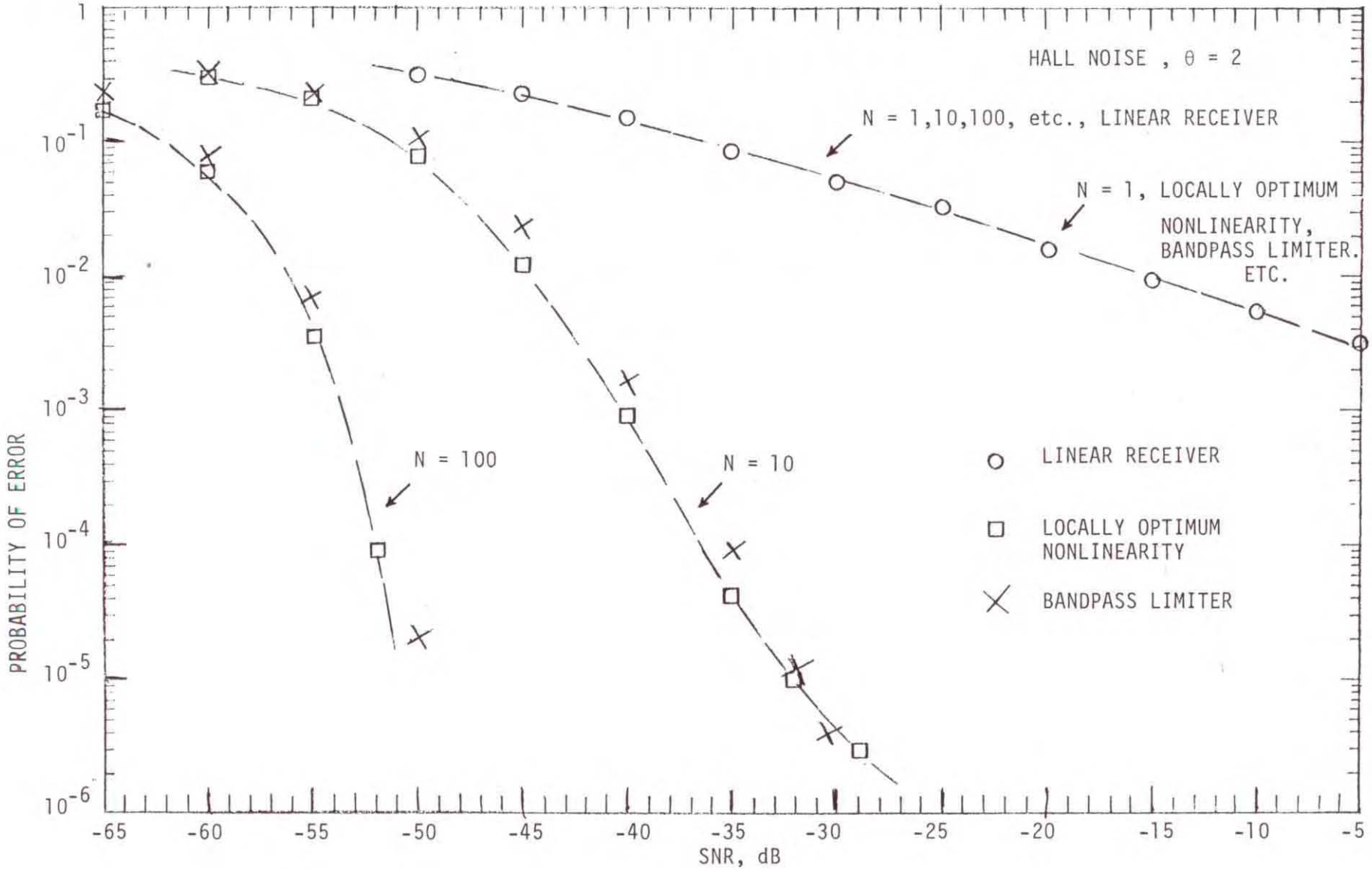

Figure 10. Simulation results with Hall noise, θ = 2, and constant signal.

$$\phi_Z(u) = \frac{2\gamma}{\pi} \int_0^\infty \frac{\gamma}{(y^2 + \gamma^2)} \cos uz \, dz = e^{-\gamma u} \quad . \tag{52}$$

So if

$$Y = \sum_{i=1}^{N} Z_i \quad , \tag{53}$$

the pdf of Y is given by

$$p_Y(y) = \frac{N\gamma}{\pi \left[y^2 + (N\gamma)^2 \right]} \quad . \tag{54}$$

That is, Y has the same pdf as the individual Z_i's, but is N times "bigger." This explains the linear receiver results of Figure 10. In doing the simulation with $\theta = 2$ and the linear receiver, a truncated Hall model was also used. That is, all values generated that were larger than some threshold were either discarded or reduced to the threshold value. This procedure made no difference and the same results shown on Figure 10 were obtained. That is, the mathematics given above still dominated. Also indicated on Figure 10 for N = 1 are results using the LOBD nonlinearity and the bandpass limiter. As indicated, these results were essentially identical to those obtained for the linear receiver, demonstrating the known result that for N = 1, no improvement can be obtained by using nonlinear receivers and in order for nonlinearities to be effective, N must be greater than 1.

Figure 11 gives simulation results for the Hall, $\theta = 2$, noise and a Rayleigh fading signal, N = 10. Note that as for a constant signal and N = 10 (Figure 6 and 10), the bandpass limiter outperforms the LOBD nonlinearity as the SNR increases. This behavior is easier to see for a Rayleigh signal, since the P_e's are much higher at the "crossover" point between the LOBD and the bandpass limiter.

To complete the simulation results for $\theta = 2$, Figure 12 shows what happens when Gaussian noise is the actual interference and our receiver uses the LOBD nonlinearity for $\theta = 2$. The solid curve is the theoretical performance for the linear receiver in Gaussian noise (optimum) and the degradation caused by using the LOBD nonlinearity (N = 10) is shown. Using (16) and (17) to compute L_{eff}, we obtain the integrals

$$L_1 = \frac{-2\theta}{\sigma^2\sqrt{2\pi\sigma^2}} \int_{-\infty}^{\infty} \frac{2}{z^2 + \gamma^2} \, e^{-z^2/2\sigma^2} \, dz \quad ,$$

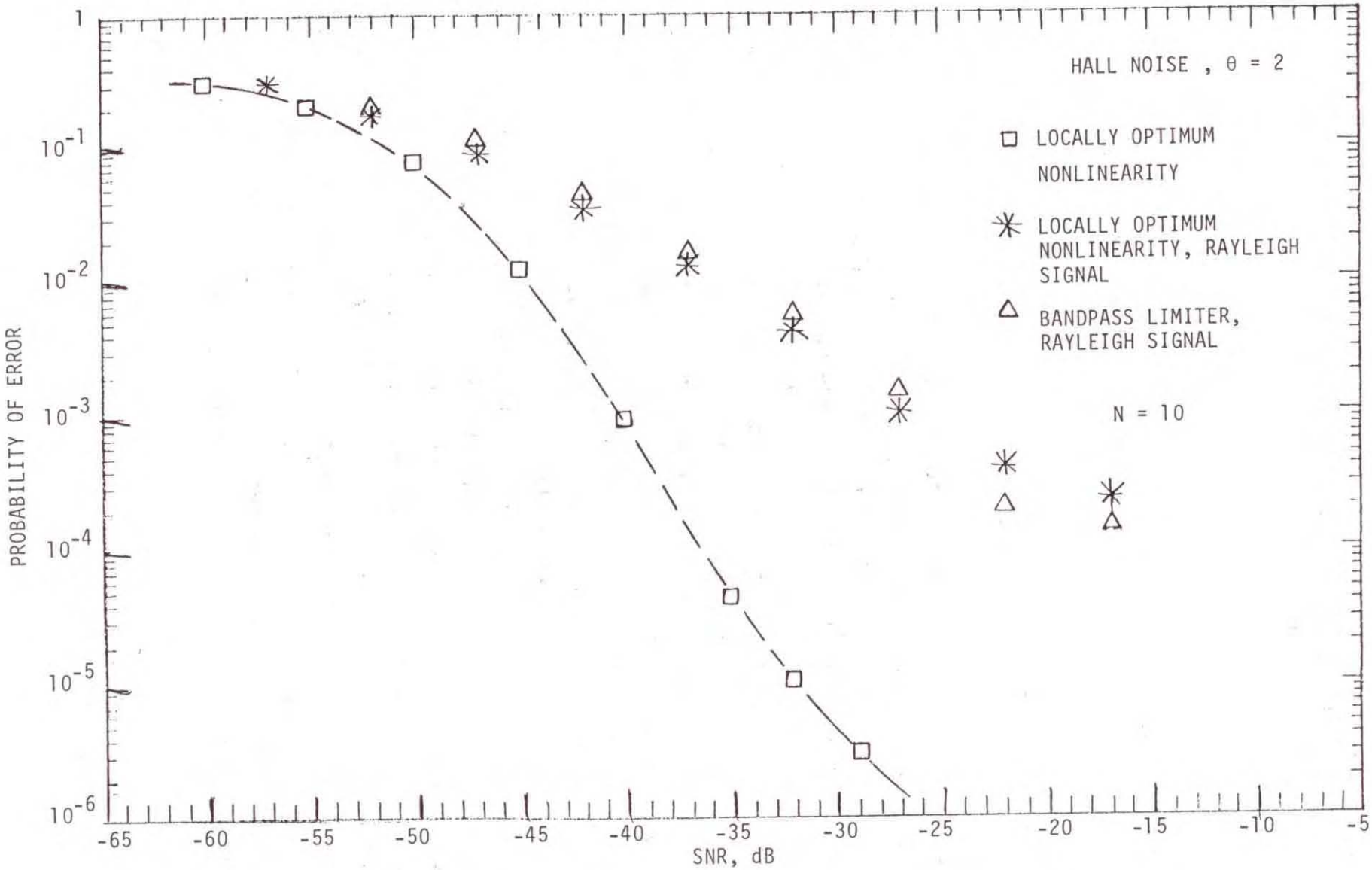

Figure 11. Simulation results for constant and Rayleigh fading signal, Hall noise, $\theta = 2$ and $N = 10$.

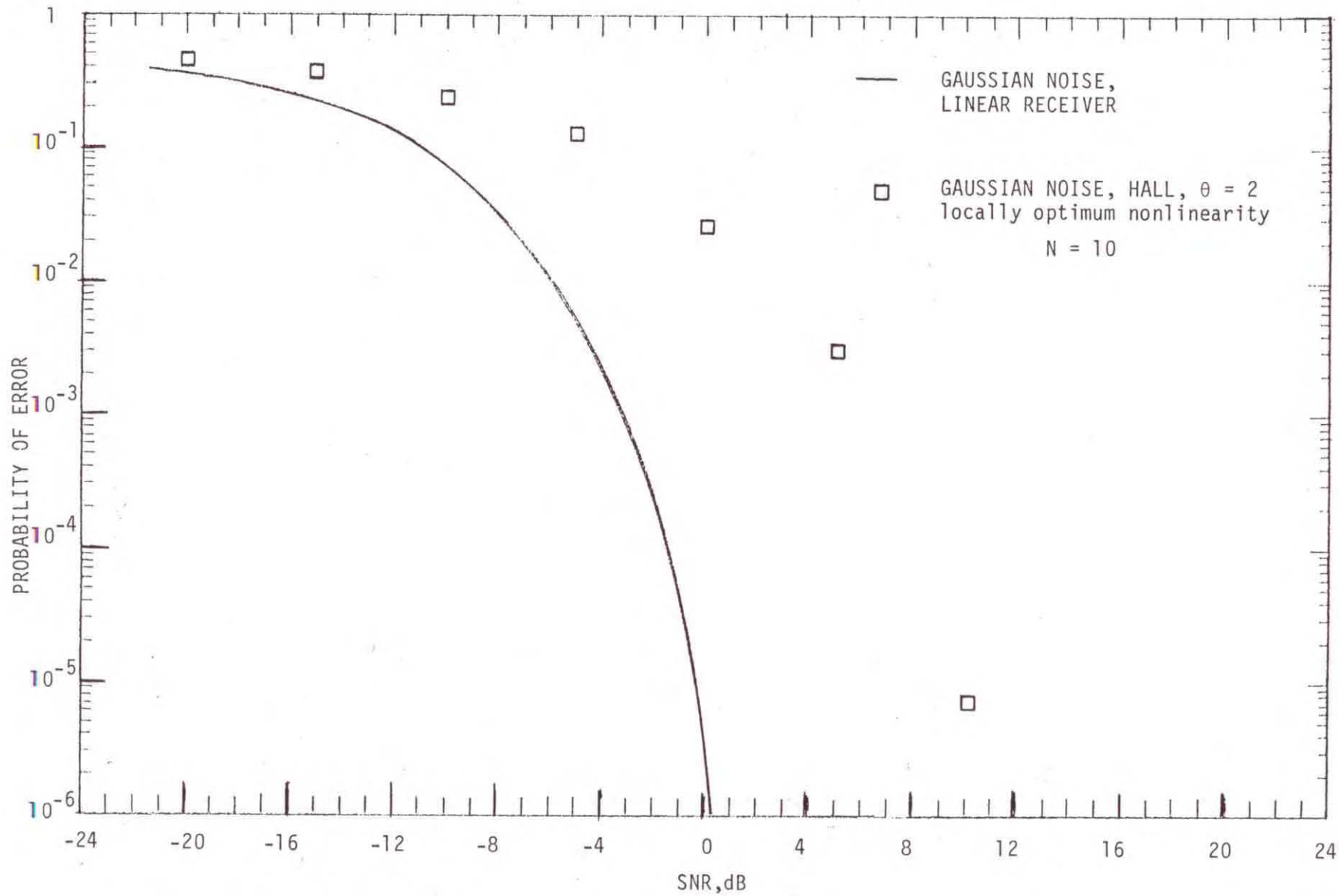

Figure 12. Simulation results for Gaussian noise into the LOBD, Hall θ = 2, nonlinearity.

and (55)

$$L_2 = \frac{2\theta^2}{\sqrt{2\pi\sigma^2}} \int_{-\infty}^{\infty} \frac{z^2}{z^2 + \gamma^2)^2} e^{-z^2/2\sigma^2} dz \quad .$$

The L_1 integral can be evaluated analytically but the L_2 apparently cannot be. Numerical integration of L_1 and L_2 gives

$$L_{eff} = L_1^2/L_2 = 0.0316 = -15.0 \text{ dB} \quad . \tag{56}$$

The L_{eff} tells us the degradation expected for "small" $S(>0)$ and $N \to \infty$. The degradation obtained for N = 10 using the simulation results is on the order of 10 dB from Figure 12. Simulation results for N = 100 were not obtained.

As detailed in Section 3, the Hall model, $\theta = 2$, properly normalized was used to approximate Middleton's model to "check" previous results based on suitably small signal and Central Limit Theorem arguments. Simulation results were also obtained for another Hall distribution, $\theta = 4$. Unlike the $\theta = 2$ case, the first three moments exist for the $\theta = 4$ case. The pdf for $\theta = 4$ is

$$p_Z(z) = \frac{2\gamma^3}{\pi(z^2 + \gamma^3)^2} \quad , \tag{57}$$

and the APD is

$$\text{Prob} \quad E > E_o = \frac{\gamma^3}{(E_o^2 + \gamma^2)^{3/2}} \quad . \tag{58}$$

If this is normalized to the envelope rms level (which now can be computed), then $\gamma = \sqrt{2}/2$. A quite interesting result is that for the Hall model, $\theta = 4$, the "improvement factor" L is only 4 (6 dB). Figure 13 shows the APD ($\theta = 4$) and this noise is obviously highly non-Gaussian. Comparing Figure 13 ($\theta = 4$) and Figure 4 ($\theta = 2$ and for which L = 37 dB), the noise distributions do not appear to be "all that much different," especially in the tails. Yet for $\theta = 4$, L is only 6 dB. As we will see from the simulation results, this "31 dB difference" (37-6) is quite real.

First, Figure 14 shows results for a linear receiver for both constant and Rayleigh fading signal. Since we are now using a "real" noise process with finite moments, we obtain "normal" results for the different time-bandwidth products. As

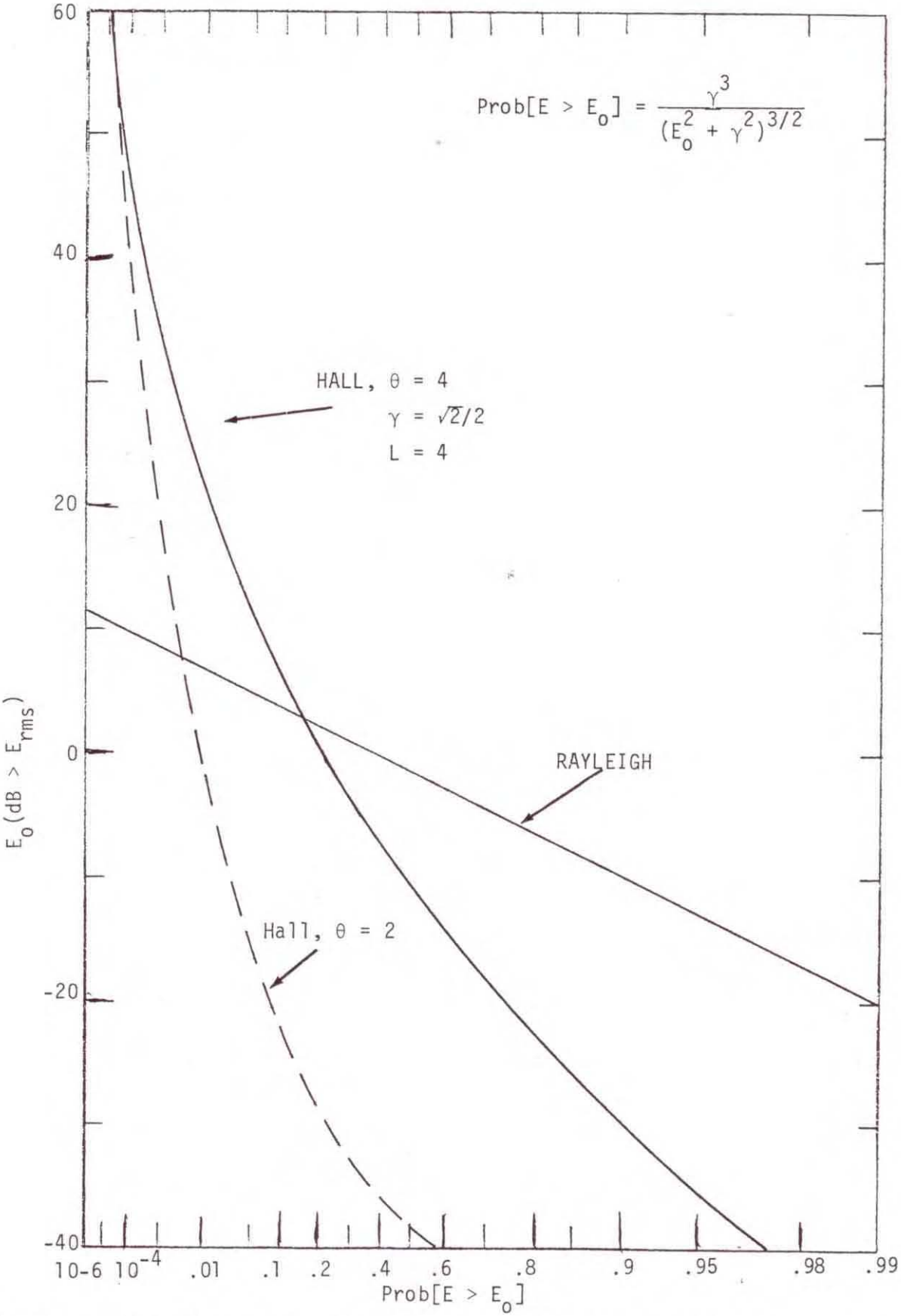

Figure 13. The Hall model APD for θ = 4. The APD is normalized to the rms envelope level.

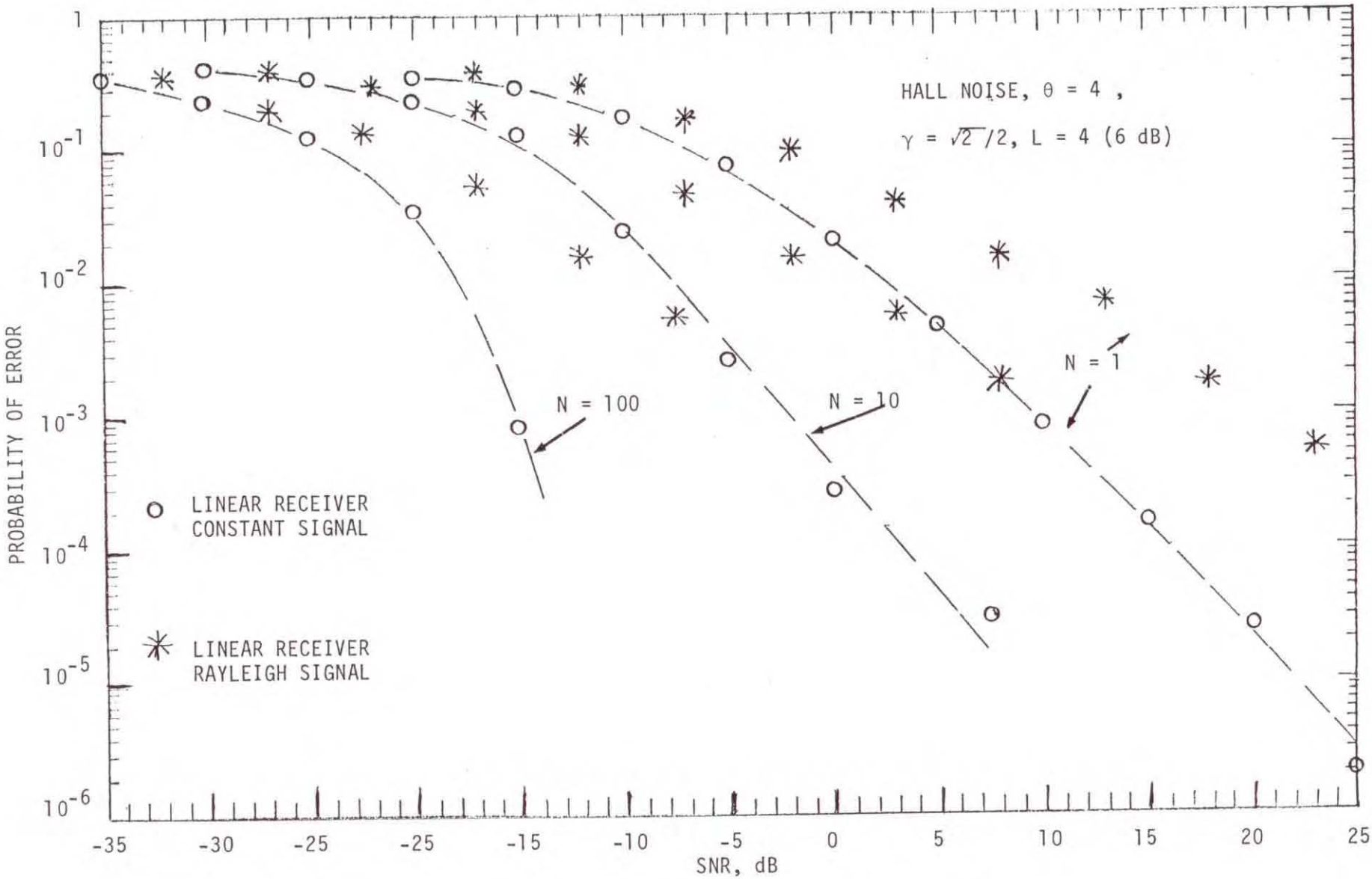

Figure 14. Simulation results for Hall noise θ = 4, and a linear receiver for both constant and Rayleigh fading signal.

Figure 14 shows, as N increases, the performance results look more and more like the standard result for Gaussian noise due to the Central Limit Theorem (which, as noted earlier, only applies to random variables with finite moments).

Figure 15 shows the linear receiver, constant signal, results along with results for the bandpass limiter and the LOBD nonlinearity. First, note that as before, use of nonlinearities for N = 1 gives no improvement over the linear receiver, but, of course, does give improvement for N = 10 and 100. For N = 100, this improvement is only 6 dB, as predicted by L. Note that the LOBD nonlinearity here also is only slightly superior to the bandpass limiter. From Figure 9 for N = 100, the linear receiver operating in Gaussian noise (optimum) requires approximately a SNR of -13 dB for $P_e = 10^{-3}$ and from Figure 15 the LOBD receiver (locally optimum) requires approximately -20 dB SNR for $P_e = 10^{-3}$. This is a 7 dB difference and the limiting difference predicted by L was 6 dB. Next, from Figure 10, N = 100, Hall $\theta = 2$ noise, a SNR of -53 dB is required for $P_e = 10^{-3}$. This is the "31 dB difference" (approximately) between the two Hall noises mentioned above and given by the two corresponding L values (37 dB versus 6 dB). This shows that we cannot arbitrarily say, by inspection, that a noise process which is "tremendously" non-Gaussian can result in "tremendous" improvement over the corresponding Gaussian or linear receiver situation.

Finally, Figure 16 compares performance for a constant signal and a Rayleigh fading signal for N = 10. Note, that while for the $\theta = 2$ case and N = 10, the bandpass limiter began to outperform the LOBD nonlinearity for both constant signal (Figures 6 and 10) and Rayleigh fading signal (Figure 11) as SNR increased. Here ($\theta = 4$) the LOBD nonlinearity appears to be "always" slightly superior to the bandpass limiter.

5. CONCLUSIONS AND DISCUSSION

In the derivation of the LOBD, two essential assumptions are made. That the desired signal is suitably small (see Middleton and Spaulding, 1983) and that the number of independent noise samples increases without limit. The usual means of estimating the performance, once the detectors have been derived, again make use of these two simplifying assumptions. This results in performance measures that are strictly true only in the limit. It has been the purpose here to investigate, via particular examples and computer Monte Carlo simulation, how the LOBD's will actually perform in actual possible operational situations. The results are varied, but in general, the "standard" limiting performance estimates do provide correct performance measures under appropriate conditions (large N and S sufficiently small).

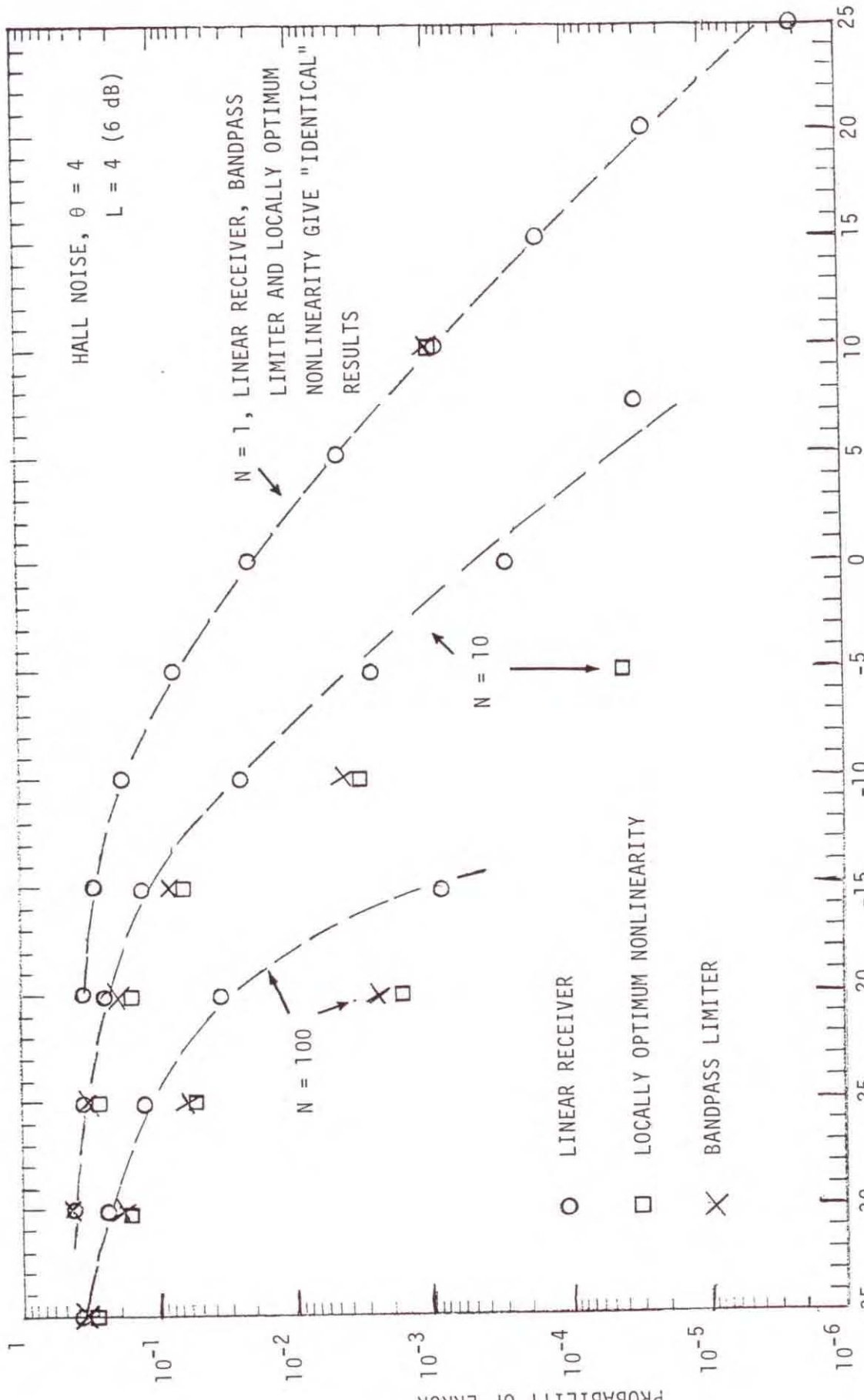

Figure 15. Simulation results for Hall noise, $\theta = 4$, for a linear receiver and for the LOBD and bandpass limiter nonlinearities.

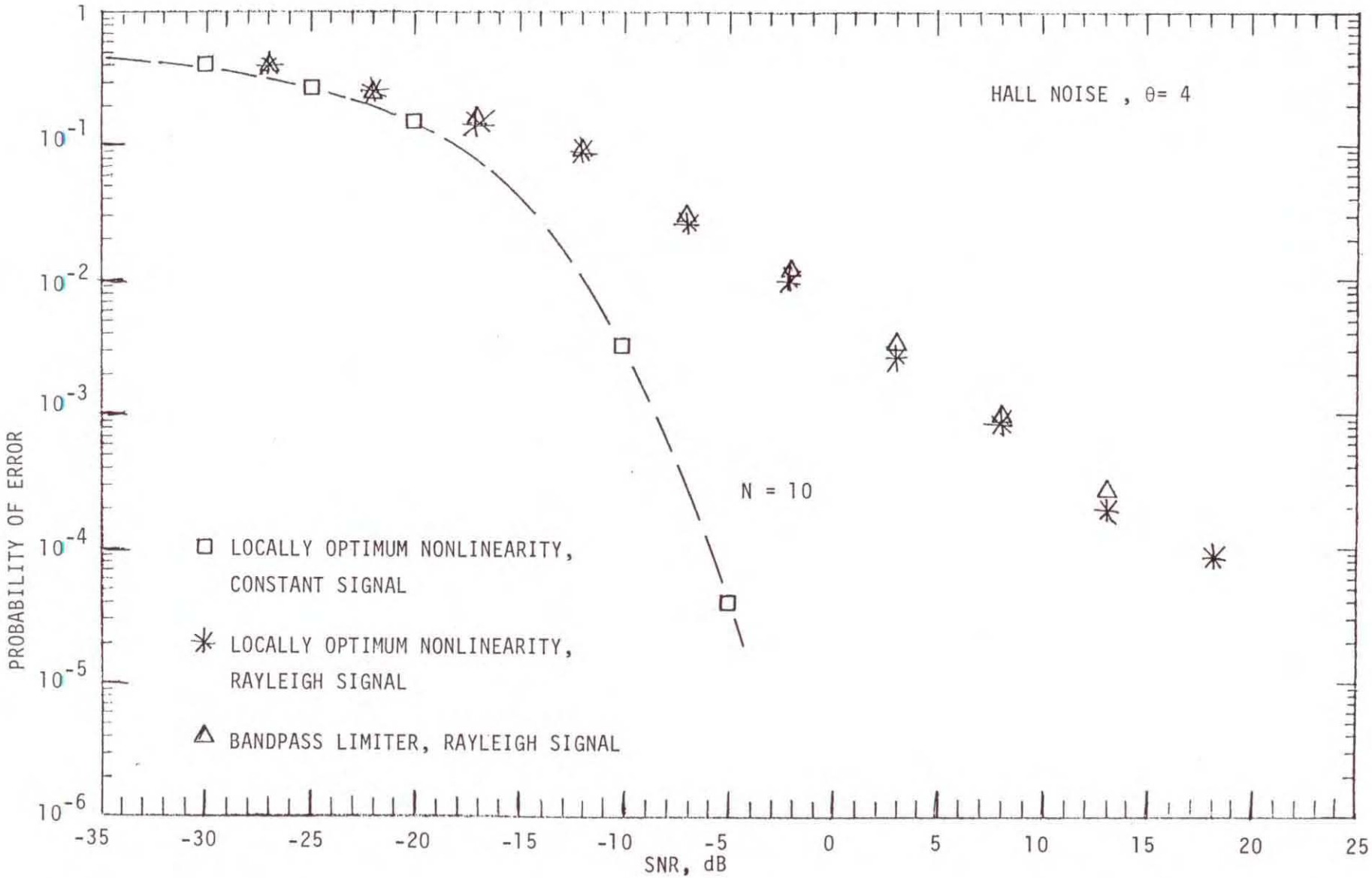

Figure 16. Simulation results for constant and Rayleigh fading signal, Hall noise, $\theta = 4$, $N = 10$.

The simulation results demonstrated that the LOBD's actually perform as advertised. One example was shown where the LOBD departed from being "close to optimum" as the signal level increased (N = 10) and was eventually outperformed by the ad hoc bandpass limiter. In all cases, the LOBD outperformed (in the limit) "reasonable" nonlinearities, e.g., the hard-limiter, only by a small amount (<3 dB) for Class B interference. The corresponding situation for Class A interference still needs to be investigated. Also, it was demonstrated that one cannot be assured of always obtaining "great" improvement over the linear receiver by using nonlinear processing. One Class B, highly non-Gaussian example (θ = 2), gave 37 dB improvement whereas another Class B, highly non-Gaussian example (θ = 4), gave only 6 dB improvement.

6. REFERENCES

Bogdan, V. M. (1981), Computer simulations of random variables and vectors with arbitrary probability distribution laws, NASA Technical Paper 1859, May.

Cahn, C. R. (1961), A note of signal-to-noise ratio in band-pass limiters, IRE Trans. Inf. Theory, pp. 39-43, January.

Davenport, W. B., Jr. (1953), Signal-to-noise ratios in band-pass limiters, J. App. Phys. 24, No. 6, pp. 720-727, June.

Davenport, W. B., and W. L. Root (1958), An Introduction to the Theory of Random Signals and Noise, (McGraw-Hill Book Co., Inc., New York).

Hall, H. M. (1966), A new model for "impulsive" phenomena: Application to atmospheric-noise communications channels, Stanford University Electronics Laboratories Technical Report No. 3412-8 and No. 7050-7, SU-SEL-66, 052.

Halton, J. H. (1970), A retrospective and prospective survey of the Monte Carlo method, SIAM Review 12, No. 1, pp. 1-63, January.

Kahn, H. and I. Mann (1957), Monte Carlo, The Rand Corporation Report P-1165, July 30.

Lu, N. H., and B. A. Eisenstein (1981), Detection of weak signals in non-Gaussian noise, IEEE Trans. Inf. Theory IT-27, No. 6, pp. 755-771, November.

Middleton, D. (1976), Statistical-physical models of man-made and natural noise Part II: First order probability models of the envelope and phase. Office of Telecommunications Report 76-86, April, 142 pp. (NTIS Acces. No. PB 253-949).

Middleton, D. (1977), Statistical-physical models of electromagnetic interference, IEEE Trans. EMC EMC-19, pp. 106-127, August.

Middleton, D., and A. D. Spaulding (1983), Optimum reception in non-Gaussian electromagnetic interference environments: II. Optimum and suboptimum threshold signal detection in Class A and Class B noise. National Telecommunications and Information Administration Report 83-120, May, 350 pp. (NTIS Acces. No. PB83-241411).

Middleton, D. (1983), Canonical and quasi-canonical probability models of Class A interference, IEEE Trans. Electromagnetic Compatibility, EMC-25, No. 2, May, pp. 76-106.

Shanmugan, K. S., and P. Balaban (1980), A modified Monte-Carlo simulation technique for the evaluation of error rate in digital communication systems, IEEE Trans. Comm. COM-28, No. 11, pp. 1916-1924, November.

Spaulding, A. D., and D. Middleton (1977), Optimum reception in an impulsive interference environment - Part I: Coherent detection; Part II: Incoherent reception, IEEE Trans. Comm. COM-25, pp. 910-934, September.

Spaulding, A. D. (1977), Stochastic modeling of the electromagnetic interference environment, Conference Record-International Communications Conference, ICC'77, Chicago, pp. 42.2-114-123 (IEEE Catalog No. 77CH 1209-6C SCB).